Microstructure and Unusual Ferromagnetism of Epitaxial SnO_2 Films Heavily Implanted with Co Ions

Rustam I. Khaibullin , Amir I. Gumarov , Iskander R. Vakhitov , Andrey A. Sukhanov , Nikolay M. Lyadov , Airat G. Kiiamov , Dilyara M. Kuzina , Valery V. Bazarov , Almaz L. Zinnatullin *

Posted Date: 4 January 2024

doi: 10.20944/preprints202401.0296.v1

Keywords: cobalt implantation; tin dioxide; microstructure; ferromagnetism; scanning electron microscopy; X-ray diffraction; X-ray photoelectron spectroscopy; vibrating sample magnetometry; ferromagnetic resonance; spintronics

Article

Microstructure and Unusual Ferromagnetism of Epitaxial SnO_2 Films Heavily Implanted with Co Ions

Rustam I. Khaibullin [1,2], Amir I. Gumarov [1,2], Iskander R. Vakhitov [1,2], Andrei A. Sukhanov [1], Nikolay M. Lyadov [1,2], Airat G. Kiiamov [2], Dilyara M. Kuzina [3], Valery V. Bazarov [1] and Almaz L. Zinnatullin [1,2,*]

[1] Zavoisky Physical-Technical Institute, FRC Kazan Scientific Centre of RAS, Kazan 420029, Russia
[2] Institute of Physics, Kazan Federal University, Kazan 420008, Russia
[3] Institute of Geology and Petroleum Technologies, Kazan Federal University, Kazan 420008, Russia
* Correspondence: almaz.zinnatullin@gmail.com

Abstract: In this work, we have studied microstructure and unusual ferromagnetic behavior in cobalt (Co)-implanted epitaxial tin dioxide (SnO_2) films. The study was aimed to provide a comprehensive understanding of the interplay between cobalt implant distribution, crystal defects, such as oxygen vacancies, and magnetic properties in Co-implanted SnO_2 films, which has potential applications in spintronics and memristor devices. The scanning electron microscopy (SEM), X-ray diffraction (XRD), X-ray photoelectron spectroscopy (XPS), vibrating sample magnetometry (VSM), differential thermo-magnetic analysis (DTMA), and ferromagnetic resonance (FMR) were employed for investigations of SnO_2 films implanted with 40 keV Co+ ions at room or the elevated temperatures of substrate. The experimental data showed that the Co ion implantation with high fluence of 1.0 10^{17} ions/cm^2 induces significant changes in the microstructure of SnO_2 films, leading to the appearance of ferromagnetism with the Curie temperature significantly above room temperature. Strong influence of implantation temperature and subsequent high-temperature annealing in air or in vacuum on magnetic properties of Co-implanted SnO_2 films were established. Moreover, the chemical effect of ethanol on FMR spectra were observed. The obtained results are discussed within the model of two magnetic layers with different concentration and valence states of the implanted cobalt and with high content of oxygen vacancies.

Keywords: cobalt implantation; tin dioxide; microstructure; ferromagnetism; scanning electron microscopy; X-ray diffraction; X-ray photoelectron spectroscopy; vibrating sample magnetometry; ferromagnetic resonance; spintronics

1. Introduction

Semiconducting tin dioxide (SnO_2) doped with a magnetic 3d-elements is a promising material for optoelectronic, photovoltaic and spintronic applications [1,2]. Although the room temperature ferromagnetism (FM) in transition metal (TM)-doped SnO_2 had been early reported ([2,3], and references therein), the origin and the mechanism of long-range ferromagnetic order are still an open question. It is often indicated that the FM strongly depends on the fabrication method of TM-doped SnO_2. Moreover, the presence of oxygen vacancies was systematically related to the observed ferromagnetic state [4–6].

The ion-beam implantation has been widely used in microelectronics for a long time as an effective method of doping classical semiconductors (Si, Ge, GaAs, etc.) with a donor or acceptor impurity [7]. Therefore, it is interesting to investigate the possibilities of ion-beam implantation for doping wide-gap oxide semiconductor SnO_2 with magnetic dopant, for example, with cobalt, with aim to create material for semiconductor spintronics. Moreover, this technique allows not only doping materials with any impurities in a wide range of concentrations, but also generates a large number of oxygen vacancies in oxide structure during the ion irradiation process [7]. The last is

 doi:10.20944/preprints202401.0296.v1

important, because, the oxygen vacancies may play a crucial role in the producing ferromagnetism in Co-doped SnO_2 as it was pointed above.

Ion implantation has already been used for doping SnO_2 films with the cobalt impurity in the concentration range of 1-7 at.% to obtain oxide-based dilute magnetic semiconductor [8–10]. However, up to now, a systematical study of Co ions implantation effect on the structure and magnetic properties of SnO_2 thin films is missing in the literature. In this work, Co ions were implanted into epitaxial SnO_2 films to high concentrations of the implanted region (more than 12 at.%). Moreover, the effect of the SnO_2 temperature during the high-fluence implantation with cobalt ions on the manifestation of ferromagnetism also was studied.

2. Materials and Methods

The experimental samples were obtained in two stages. At the first stage, thin $SnO_{2-\delta}$ films with a thickness of 140-150 nm were grown on C-cut Al_2O_3 single crystalline substrates (15.0 × 15.0 × 1.0 mm^3 in sizes) by the reactive ($Ar+O_2$) magnetron sputtering of the elemental tin target. The subsequent annealing in air at the temperature of 1273 K for 120 min has been performed to recover the stoichiometric oxygen content in the films. As a result, epitaxial SnO_2 films were obtained. Then, at the second stage, 40 keV Co^+ ions were implanted into epitaxial SnO_2 films to the fluence of 1.0 × 10^{17} ion/cm^2 at an constant ion current density of 2-3 μA/cm^2. The implantation was performed by using *ILU-3* ion-beam accelerator (ZPTI FRC KSC of RAS, Russia) at different temperature of substrate (film) during ion irradiation – either at room temperature (**sample CoSO-1**) or at the elevated temperature of 750 K (**"hot"** implantation, **sample CoSO-2h**). Additionally, one SnO_2 epitaxial film was implanted with 40 keV ions of inert gas (argon) to same fluence at the elevated substrate temperature (**sample ArSO-3h**). The last sample was found to be useful to establish microstructure changes without inducing the ferromagnetism and, thus, to determine the nature of ferromagnetism in the Co-ions implanted samples. The SnO_2 sputtering induced by intensive ion irradiation was taken into account. The steps between the implanted and pristine regions of the oxide film were measured using the *DektactXT* profilometer (Bruker Nano GmbH, Berlin, Germany). The sputtering coefficient was calculated to be equal to $\alpha \approx 3.78$ or 5.16 atoms/ion considering the sputtered step heights of about 45 nm or 62 nm in SnO_2 films implanted at room or elevated substrate temperatures, samples CoSO-1 and CoSO-2h respectively. The small parts (~3.0 × 3.0 × 1.0 mm^3 in sizes) of Co-ions implanted SnO_2 films were annealed firstly at the high-temperature of $T_{ann.} = 873$ K for 30 minutes in an air atmosphere. After measuring their magnetic properties, these parts of the samples were subjected to a second annealing under high vacuum conditions (10^{-6} Torr) at the same temperature of 873 K and time of 30 minutes. These annealed samples are marked by the suffix "av" as **CoSO-1_av** and **CoSO-2h_av**, respectively.

The phase composition and crystal structure of SnO_2 films before and after Co-ions implantation were investigated by X-ray diffraction (XRD) method using *Bruker D8 Advance* diffractometer where X-ray tube with the Cu-Kα anode (λ=0.15418 nm) was mounted. Surface morphology and element composition of both as-prepared and the implanted SnO_2 films were investigated by using an *EVO 50 XVP* scanning electron microscope (SEM) (Carl Zeiss AG, Oberkochen, Germany) equipped with an energy-dispersive X-ray (EDX) spectrometer (Oxford Inca Energy-350, Oxford Instruments, Abingdon, England).

The valence state of the elements and their distribution at various depths of the sample were examined using X-ray photoelectron spectroscopy (XPS) employing ion etching technique. The step-by-step etching process was conducted utilizing a 2 keV Ar^+ ion beam. The *Bruker DektakXT* profilometer was employed to control the depth profile differences between the etched and non-etched regions. After each etching session, XPS spectra were recorded using a *Phoibos 150* hemispherical energy analyzer (SPECS GmbH, Berlin, Germany). The obtained results were analyzed using CasaXPS software [11].

Magnetic properties of the Co-implanted SnO_2 films were studied using the VSM magnetometry, ferromagnetic resonance and the differential thermo-magnetic analysis methods. The magnetization curves were recorded on a home-made rotating sample magnetometer [12] by scanning the magnetic

Preprints (www.preprints.org) | NOT PEER-REVIEWED | Posted: 4 January 2024 doi:10.20944/preprints202401.0296.v1

field up to 5 kOe in the plane of the samples (in-plane measurement geometry) at room temperature. The diamagnetic contribution of the Al_2O_3 substrate was subtracted after the magnetic measurements, and the value of the measured magnetic moment was normalized to the area of specimens under magnetic study in order to calculate the magnetization per implanted cobalt atom.

Ferromagnetic resonance (FMR) spectra of samples under study were taken on a *Bruker ElexsysE580* (Bruker GmbH, Berlin, Germany) X-band spectrometer (9.64 GHz) at room temperature. The angular dependences of the FMR spectra were recorded by rotating of the applied DC magnetic field in plane perpendicular to the sample plane ("out-of-plane" geometry). As usually the first field-derivative of microwave power absorption (dP/dB) was recorded as a function of static magnetic field (B). The value of the resonant field ($B_{res.}$) was determined by the intersection point of the magnetic resonance curve with the baseline of the empty resonator.

The thermo-magnetic curves were measured using the Faraday balance technique [13] by heating samples from 300 to 1000 K with the rate of 100 K/min in air at applied field of 500 mT.

3. Results and Discussion

3.1. X-ray Diffraction (XRD) Analysis

The results of X-ray diffraction studies are presented in Figure 1. The θ-2θ scan pattern of the epitaxial SnO_2 film grown on C-cut Al_2O_3 substrate is shown in Figure 1a by the green curve. The sharp diffraction peaks observed at 2θ angles of ~41.9° and ~91° may be unambiguously attributed to the (0006) and (000 12) reflections from the C-cut Al_2O_3 substrate. Two other peaks at 2θ angles of ~37.9° and ~80.6° were assigned to (200) and (400) reflections from the SnO_2 film. The last proves out-of-plane epitaxial relationship for SnO_2 film on C-cut Al_2O_3 substrate as $SnO_2(200) \parallel Al_2O_3(0006)$.

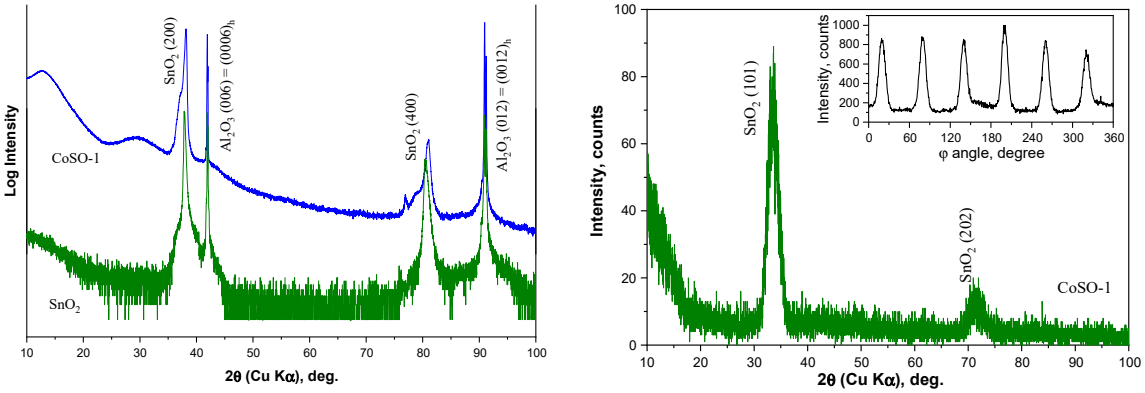

Figure 1. The results of X-ray diffraction studies of the epitaxial SnO_2 film on C-cut Al_2O_3 substrate before and after Co-implantation: (**a**) – θ-2θ scans of the film before (green curve) and after (blue curve) implantation; (**b**) – θ-2θ scan of the film before implantation under fixed angles of ψ = 56.2° and φ = 79.9°. The inset in (**b**) shows the φ-scan of the (101) reflection for the film before implantation (2θ = 33.7° and ψ = 56.2°).

To confirm the epitaxy of the synthesized SnO_2 films, the φ-scan of the (101) reflection was performed under tilt angle of ψ = 56.2° and 2θ = 33.7° (see inset in Figure 1b). The sixfold symmetry was discovered in this pattern that is not consisted with the tetragonal rutile structure since twofold symmetry should be characteristic for (101) reflections. The observed sixfold symmetry may be associated with the formation of three equivalent domains during the growth of SnO_2 films. The same result has been reported earlier [14]. In Figure 1b, the θ-2θ scan pattern of the SnO_2 film before implantation under fixed angles of ψ = 56.2° and φ = 79.9°. This picture also confirms the phase purity and the epitaxy of the synthesized SnO_2 films.

The XRD pattern of the Co-implanted SnO_2 film is shown in Figure 1a by the blue curve. One may observe that, on the one hand, the position of the SnO_2 related reflexes were slightly shifted toward higher 2θ angles and, on the other hand, the shoulders were appeared in the lower angle

sides of the each (200) and (400) peaks. For the SnO_2 implanted at the elevated temperature, qualitatively same XRD pattern was obtained. We suppose the following model in order to explain the both experimental facts.

Under the high-fluence implantation, initially uniform in depth SnO_2 films were separated into two layers. In the first layer, located closer to the film surface, there is the highest concentration of the implanted ions that is also confirmed by the results of XPS analysis as will be shown below. The notably part of cobalt atoms form precipitates in this layer. These precipitates may stretch the SnO_2 matrix and, therefore, an enhance in the lattice spacings may be expected due to them. Thus, the shoulder-like reflexes in the lower angle sides of SnO_2 reflexes may be originated by the cobalt precipitates.

In the second layer, cobalt impurity, according XPS results, in the 2+ valence state substitutes Sn^{4+} sites in the SnO_2 structure. According to the previous studies, Co^{2+} ions substitute Sn^{4+} ions in the low-spin state [15,16]. Since the ionic radius of low-spin Co^{2+} ions are smaller than Sn^{4+} in the sixfold oxygen environment (0.65 Å and 0.69 Å, respectively [17]), such substitution should decrease the lattice parameters and, therefore, reduce the lattice spacings. The last should results in the shift of XRD peaks towards higher angles. Moreover, some decrease in the lattice parameters may be due to the decrease in the film thickness since the thickness of the Co-implanted SnO_2 film is smaller in compare with the virgin state due to surface sputtering during the ion implantation process. Indeed, the reduction of the lattice parameters with the decrease in film thickness was reported for the epitaxial SnO_2 films on C-cut Al_2O_3 [14].

3.2. Scanning Electron Microscopy (SEM)

Surface topography and elemental composition of both as-prepared and the implanted SnO_2 films were studied in detail by SEM methods. The SEM analysis revealed significant changes in the morphology of the SnO_2 films upon cobalt (or argon) ion implantation. The as-prepared SnO_2 film had a smooth and compact surface (see Figure S1 of the Supplementary Material), while the cobalt-implanted films exhibited the presence of neoplasms scattered uniformly on the surface. As it is shown in Figure 2, these neoplasms have a semi- spherical form with the sizes in the range of 40-120 nm. Note that the neoplasms formation cannot be associated with the precipitation of cobalt impurities on the surface of Co-implanted samples, since exactly the same neoplasms were observed on the surface of SnO_2 film implanted with argon ions (see Figure S2 of the Supplementary Material). This also cannot be attributed to metallic tin nanoparticles, since our XPS analysis and Mössbauer studies showed that the tin atoms in the SnO_2 films are in the 4+ valence state both before and after ion implantation (Figures S4 and S5 of the Supplementary Material). Moreover, EDX element mapping taken at submicron scale (see Figure S1 of the Supplementary Materials) shows that both cobalt implant and the tin are homogenously distributed over the surface of the implanted SnO_2 films without any regions with higher content of both chemical elements. Thus, the observed morphological changes have been related to radiation defects and structural distortions in the SnO_2 lattice, leading to microscale swelling of surface. The formation of a developed relief on the surface of oxide materials as a result of high-fluence implantation is a typical case [18], and often it is associated with the processes of release of gaseous elements (oxygen) from the surface region of the irradiated material [7].

Preprints (www.preprints.org) | NOT PEER-REVIEWED | Posted: 4 January 2024 doi:10.20944/preprints202401.0296.v1

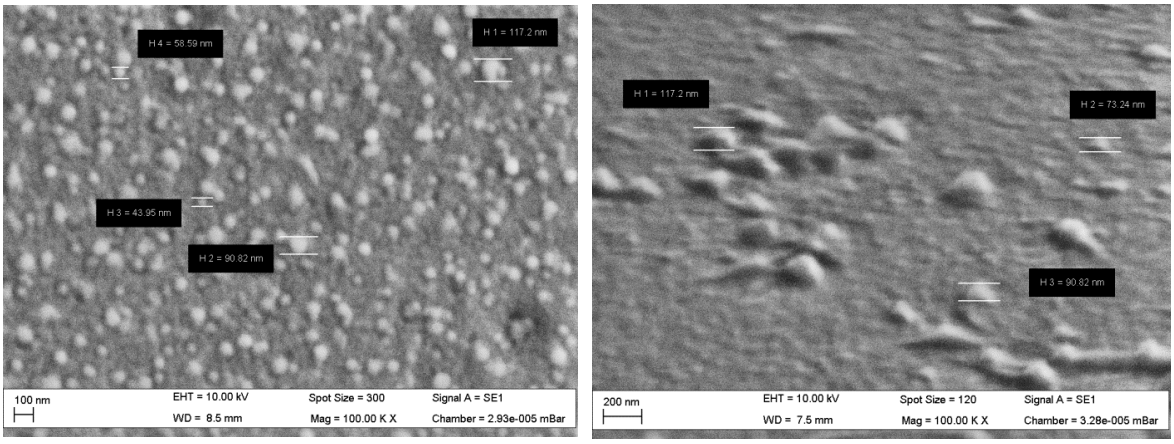

(**a**) (**b**)

Figure 2. SEM image of the surface of SnO_2 film after implantation of Co ions with the fluence of 1×10^{17} ion/cm^2 **(a)** and SEM image of same film under 70˚ degrees position **(b)**.

The chemical elements content in the studied SnO_2 samples were estimated from the EDX microanalysis data, and their values are given in Table 1. It is important to note that the Table shows the mean values of the atomic concentration of each chemical element, obtained as a result of averaging the thickness of the layer in which the characteristic X-ray radiation is generated during EDX measurements. According to our calculations within the framework of the CASINO program [19], for an electron beam energy of 5 keV used to record the EDX spectra, the thickness of the generation layer of the K-lines (Al and O) and L-lines (Sn and Co) is approximately equal to 110-120 nm. This value is close to the thickness of the implanted SnO_2 films (~ 90-100 nm) taking into account the sputtering of films during ion implantation.

Table 1. Chemical elements content in both as-prepared SnO_2 film and SnO_2 films implanted with Co (or Ar) ions at the fluence of 1×10^{17} ion/cm^2. Here T_{imp} and T_{ann} in second column show the values of the implantation temperature and temperature of subsequent double annealing in an air and then in vacuum, respectively.

Sample	$T_{imp.}/T_{ann.}$ (K)	Co (L_α, at.%)	Sn (L_α, at.%)	Al (K_α, at.%)	O (K_α, at.%)	Sn/Al	Co/Sn
SnO_2	- / 1273	-	28.8	0.8	70.4	36.0	-
CoSO-1	300/ -	14.1	22.1	3.0	60.8	7.4	0.6
CoSO-1_av	300 / 873	12.4	20.8	5.4	61.4	3.9	0.6
CoSO-2h	750 / -	12.1	22.9	3.1	61.9	7.4	0.5
CoSO-2h_av	750 / 873	11.5	21.7	3.9	62.9	5.6	0.5
ArSO-3h	750 / -	3.4 (Ar)	25.5	2.6	68.5	9.8	-

EDX elemental microanalysis confirms the successful implantation of Co ions into the SnO_2 films with an average concentration value of 12-14 atomic %. The chemical formula of Co ions implanted samples can be written as $Sn_{(1-x)}Co_xO_{2-\delta}$. The concentration ratio of cobalt to tin (column Co/Sn) allows to determine cobalt dopant content (x) in the films as $x \cong 0.38$ in the sample implanted at room temperature and $x \cong 0.33$ in sample implanted at high temperature of 750 K. As follows from the Table data, the content of structure-forming elements, tin (Sn) and oxygen (O), is significantly reduced in Co- or Ar - implanted SnO_2 films when compared with as-prepared SnO_2 film. These data confirm the fact of film sputtering during ion implantation. The sputtering process of SnO_2 film during ion irradiation is also indicated by a significant decrease in concentration ratio of tin to aluminum (column Sn/Al). The Sn/Al ratio decreases from 36.0 in as-prepared film to 7.4 in Co-implanted films and to 9.8 in Ar-implanted sample. Here, the EDX signal from Al comes from the corundum substrate (Al_2O_3) used for SnO_2 film growth. Moreover, the Sn/Al ratio continues to

Preprints (www.preprints.org) | NOT PEER-REVIEWED | Posted: 4 January 2024 doi:10.20944/preprints202401.0296.v1

decrease in the samples after high-temperature annealing, which indicates the evaporation of part of the implanted SnO_2 material during the double heat treatment of samples.

3.3. X-ray Photoelectron Spectroscopy (XPS)

The experimental cobalt impurity concentration values at various depths, derived from XPS analysis of implanted SnO_2 films at room (300 K) or the elevated (750 K) substrate temperatures, are illustrated at Figure 3a,b, respectively. The dashed line in the figures shows the distribution profile of cobalt atoms, calculated using the SRIM algorithm considering the sputtering of the part of SnO_2 film during ion irradiation [20,21]. The calculated profile exhibits half-bell-shaped distribution with concentration maximum (~26 at. %) on the surface of sample. The experimentally observed cobalt concentration profile in the implanted at room temperature sample (Figure 3a) has almost same depth distribution differing only by shift in depth (4 nm) of concentration maximum and its higher (~32 at. %) value in the comparison with the SRIM profile. In contrast, "hot" implantation (Figure 3b) lead to much wider depth distribution (up to 60 nm) of cobalt impurity and notably lower maximum concentration (~14 at. %). We associate this long "tail" in the measured cobalt distribution with diffusion blurring of the impurity distribution profile caused by high temperature of substrate during ion implantation process.

High-resolution Co *2p* spectra at different etching depths were decomposed into components. For visual clarity, the Co $2p_{3/2}$ binding energy regions are presented on Figure 3c,d. The recorded XPS spectra of cobalt can be decomposed into two components. The values of binding energies of the components are 777.9 eV – Co^0 and 781.1 – Co^{2+} [22,23]. Moreover, observable satellite feature of Co *2p* spectrum at ~786 eV enable to distinguish Co oxidation state as Co^{2+}. A comprehensive analysis of the obtained XPS data allow to establish a distribution of both the concentration and valence states of the cobalt impurity in the irradiated SnO_2 layer. These curves are shown in Figure 3a,b. As it can be seen in Figure 3a for cobalt implanted SnO_2 film at room temperature of substrate, the implanted impurity is represented by a mixture of metallic and oxidized divalent states. The metallic Co^0 component dominates at the maximum (~5 nm) of impurity distribution. Consequently, herein implanted impurity is obviously in the form of nanoparticles of metallic cobalt due to its high atomic concentration at the peak of distribution function. On the contrary, a significant part of the cobalt is in the oxidized divalent state in the tail of impurity distribution. In the case of "hot" implantation, Co^{2+} component is dominant throughout the entire depth of impurity distribution. Thus, the impurity can be found in the form of metallic nanoparticles of cobalt as well as in the form of Co^{2+} ions, which are substitute Sn^{4+} sites in the SnO_2 matrix. It should be noted that according ^{119}Sn Mössbauer results tin atoms preserve its 4+ state after implantation (see Figure S4 in Supplementary Information).

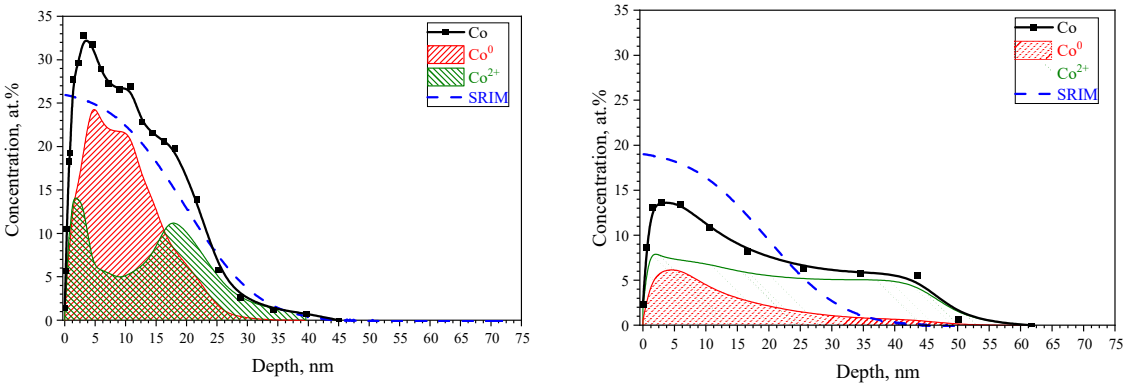

Preprints (www.preprints.org) | NOT PEER-REVIEWED | Posted: 4 January 2024 doi:10.20944/preprints202401.0296.v1

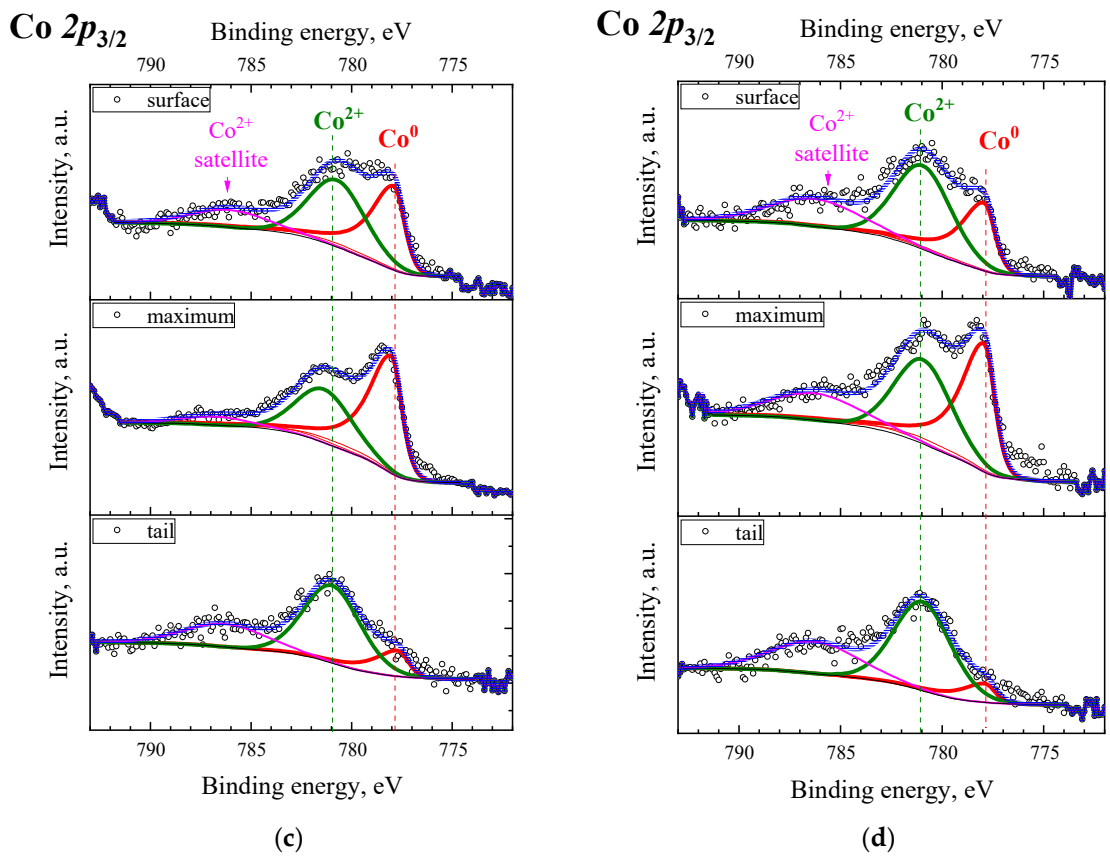

Figure 3. Depth distribution profiles of the cobalt implant (upper panel) and high resolution XPS spectra (bottom panel) recorded at the different depths of analysis for SnO_2 films implanted at room (300 K) – (*a*) and (*c*) or the elevated (750 K) – (*b*) and (*d*) substrate temperatures, respectively. The dashed lines on (*a*) and (*b*) show the theoretical distribution profiles of impurity, calculated using the SRIM algorithm [20] and the substrate sputtering during the ion irradiation [21].

3.4. Magnetic properties

The magnetic hysteresis loops recorded at room temperature for Co-ion implanted SnO_2 films both keeping the substrates at room temperature (blue curve) and at the elevated temperature of 750 K (red curve) are depicted in Figure 4a. It is clearly seen that the samples show pronounced ferromagnetic response. However, the parameters of loops notably differ between each other. Considering the SnO_2 film implanted with Co ions at the elevated substrate temperature, the saturation magnetization value is higher than for the other sample (~0.95 μ_B per implanted Co ion (μ_B/Co) vs. ~0.55 μ_B/Co). At the same time, the coercivity has opposite behavior, namely, its value in the case of the Co implantation into SnO_2 film at the elevated substrate temperature is lower than in the case of the implantation at room temperature of substrate (~400 Oe and ~2500 Oe, respectively). The coercivity for SnO_2 film implanted with Co ions at room temperature is very high and, to our best knowledge, close values have not been reported yet for Co-doped SnO_2 systems. We suppose that such unexpected large coercivity is due to the formation of oriented metallic Co nanoparticles and, probably, due to shape anisotropy of this particles. However, additional high-resolution transmission electron microscopy studies are required to prove our assumption.

In Figure 4b thermo-magnetic curves for both samples are shown. It is easily seen that the thermal behavior of samples significantly differs. Considering the curve for SnO_2 film implanted with Co ions at room temperature (blue curve), the two steps of the "magnetization removal" may be observed in the regions of ~570-730 K and ~730-900 K. At the same time, for the second sample, there is only single step mainly located in the first temperature region.

Preprints (www.preprints.org) | NOT PEER-REVIEWED | Posted: 4 January 2024 doi:10.20944/preprints202401.0296.v1

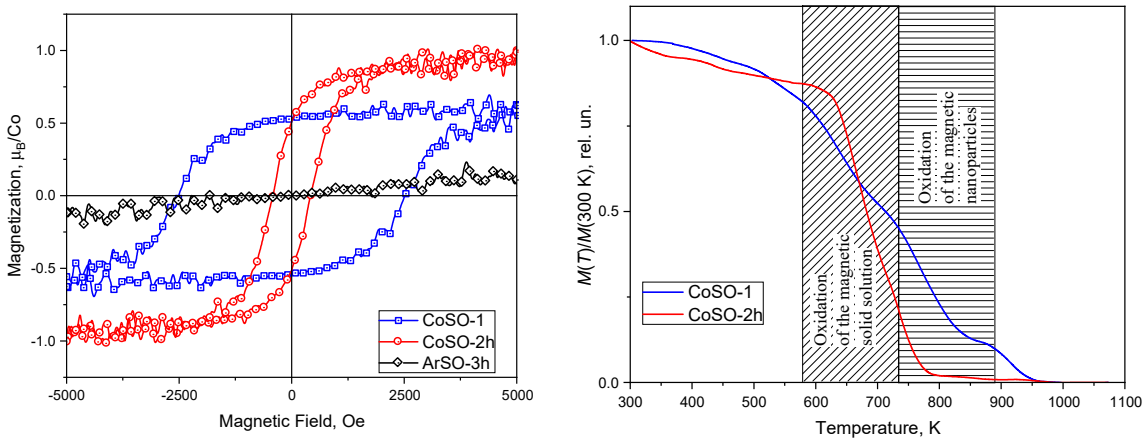

(**a**) (**b**)

Figure 4. (**a**) – Room-temperature ferromagnetic hysteresis loops for SnO_2 films implanted with Co ions keeping substrates at room temperature (blue squares) and elevated temperature (red circles). The paramagnetic curve of SnO_2 film implanted with Ar ions at elevated substrate temperature is shown by black rhombs. (**b**) – DTMA curves for same Co-ions implanted films. Patterned regions in (**b**) show the specific oxidation conditions for the various sources of ferromagnetism established in the studied samples.

Air and vacuum thermal annealing of Co-implanted SnO_2 films were performed to investigate the role of oxygen vacancies (V_O) on the manifestation of ferromagnetism. Due to the low formation energy of oxygen vacancies [24], their number in the sample can be easily controlled by changing the annealing environment. It is well known (see e.g., [25]) that the oxidizing atmosphere of air compensated the oxygen vacancies in the SnO_2-based nanomaterials while the vacuum annealing resulted in the increase in the concentration of oxygen vacancies. The Figure 5 shows the magnetization curves of both as-implanted samples (CoSO-1 and CoSO-2h) and the same samples annealed in air and then subsequently in vacuum. The annealing in air at 873 K almost totally remove the ferromagnetism for both samples. At the same time, we show that after the subsequent annealing in vacuum at 873 K the ferromagnetism may be recovered. However, the magnetic characteristic of recovered ferromagnetic loop for SnO_2 film implanted with Co ions at room temperature of substrate is strong different in compare with one in the initial state, namely, the coercivity is ~70 Oe after the vacuum annealing instead of ~2500 Oe in the initial state. Considering the sample implanted at the elevated substrate temperature, the magnetic characteristics of sample after vacuum annealing are almost comparable with the values in its initial state. Thus, the above results of our magnetic measurements indicate a crucial role of oxygen vacancies in producing ferromagnetism in Co-implanted SnO_2 films.

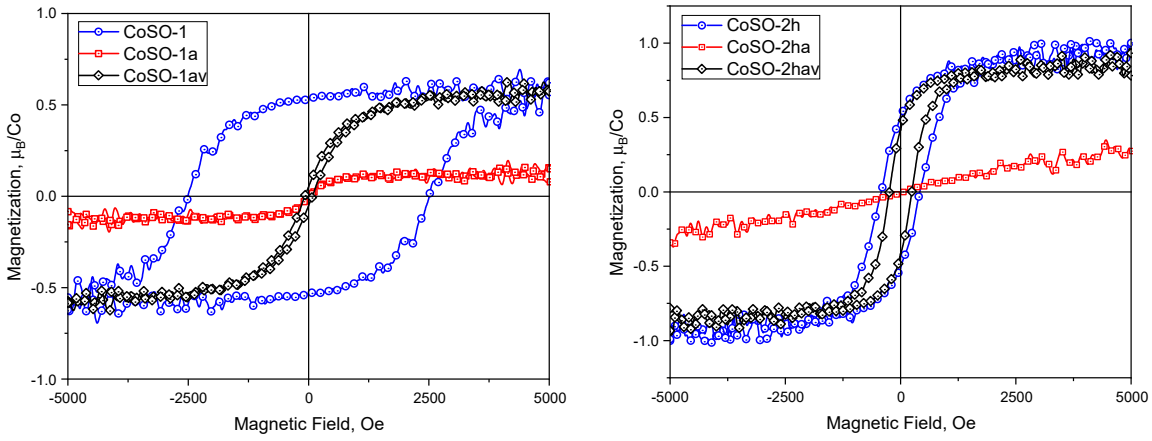

(**a**) (**b**)

Preprints (www.preprints.org) | NOT PEER-REVIEWED | Posted: 4 January 2024 doi:10.20944/preprints202401.0296.v1

Figure 5. Room-temperature ferromagnetic hysteresis loops for SnO_2 films implanted with Co ions keeping substrates at room temperature (**a**) and elevated temperature (**b**) recorded in the initial state of samples (blue curves), after annealing at 873 K in air (red curves), and after subsequent vacuum annealing at 873 K (black curves).

3.5. Ferromagnetic resonance (FMR)

3.5.1. FMR spectra

Figure 6a,b show the magnetic resonance spectra recorded at different values of the polar angle θ in CoSO-1 and CoSO-2h samples. Three FMR signals are clearly observed in the magnetic resonance spectra at the limiting value θ = 0° when magnetic field is perpendicular to the sample plane. The first two FMR signals marked with a blue triangle and a red circle in Figure 6a,b reveal a strong out-of-plane angular dependence of FMR signal positions. Namely, these two signals quickly shift from the high-field part to the low-field part of magnetic spectrum and broaden with increasing polar angle value. On the other hands, the third signal marked with a black square has a weak angular dependence in the SnO_2 film implanted with Co ions at the elevated substrate temperature during implantation (Figure 6b). The angular dependence of third signal is totally absent in the SnO_2 film implanted with Co ions at room temperature of substrate as seen in Figure 6a.

The angular dependences were analyzed by fitting the experimental spectra with the sum of three independent FMR lines. The observed lines were described by the Dyson shape line [26]. To fit the experimental spectra, a program was written in Python using the SciPy library [27]. From fitting FMR spectra, resonance field values were obtained for three lines at different orientations of the samples in the magnetic field. The angular dependencies of resonance fields are presented in Figure 6c,d for Co-implanted SnO_2 film implanted with Co^+ ions at room and high temperatures, respectively. A detailed analysis of the observed angular and temperature (not shown) dependences of the ferromagnetic resonance spectra and determination of the spectroscopic and magnetic parameters of the samples, such as the values of the g-factor, magnetization and magnetic anisotropy constants, is the subject of a separate article. At this stage, however, it can be noted that the angular dependences of the resonant field of the first two FMR signals presented in Figure 6c,d are typical for thin granular magnetic films with strong magnetic anisotropy [28,29]. On the contrary, the weak angular dependence of the third signal is characteristic of isotropic bulk ferromagnetic materials.

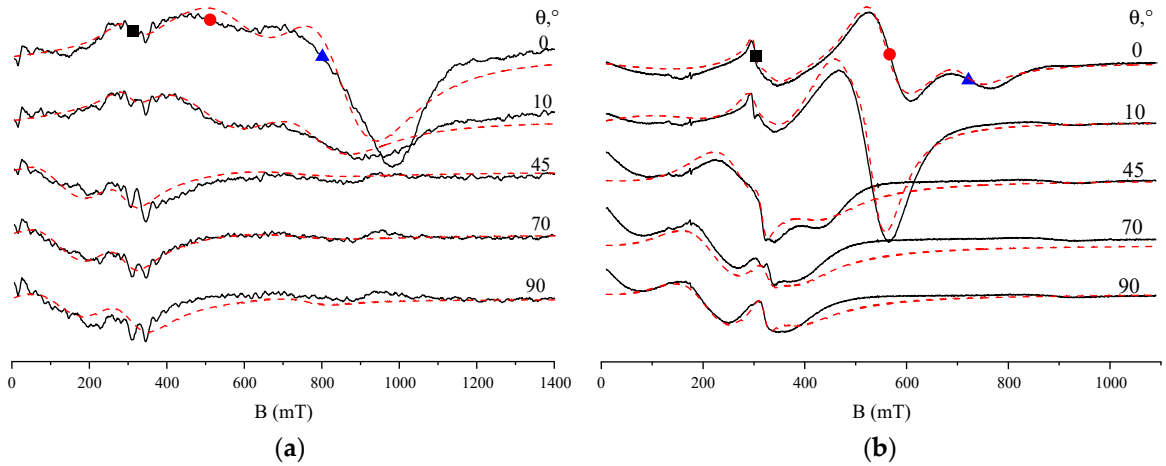

Preprints (www.preprints.org) | NOT PEER-REVIEWED | Posted: 4 January 2024 doi:10.20944/preprints202401.0296.v1

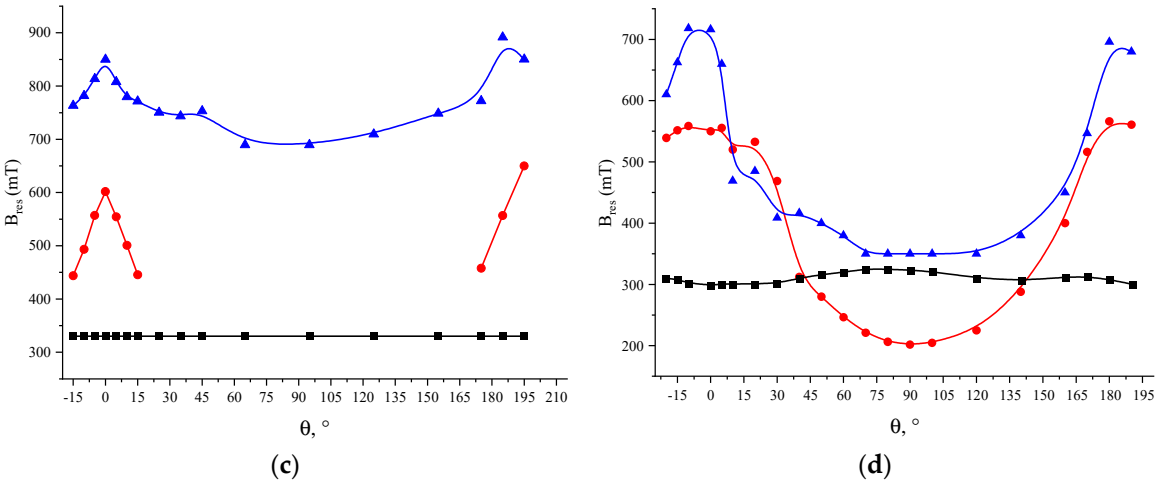

Figure 6. *Upper panel* – Room-temperature FMR spectra for various orientations of the magnetic field in CoSO-1 (**a**) and CoSO-2h (**b**) samples. Here θ is angle between a magnetic field and the normal to the sample plane ("out-of-plane" geometry). The black and the red dashed lines show experimental and simulation spectra, respectively. *Lower panel* - Angular dependences of resonance fields (B_{res}) for three FMR signals in CoSO-1 (**c**) and CoSO-2h (**d**) samples, respectively.

3.5.2. Chemical effect of ethanol on FMR spectra

The strong influence of ethanol media on the FMR was observed for first time. This chemical effect of ethanol is shown in the example of influence of storage the Co-implanted SnO_2 film in ethanol media on the FMR spectrum. It should be noted that this effect was observed for samples subjected to double annealing firstly in an air and then in vacuum at temperature of 873 K for 30 min. The FMR spectrum of CoSO-2h_av sample is shown in Figure 7. For this spectrum (in Figure 7 labeled as "Initially"), an angular dependence was observed (not shown here) similar to observed in the as-implanted CoSO-2h sample (Figure 6b). After keeping the sample in ethanol for more than 2 hours, the FMR spectrum is totally disappeared (in Figure 7 labeled as "After Ethanol"). Then, the CoSO-2h_av sample was annealed in vacuum again, the FMR spectrum is recovered (in Figure 7 labeled as "Recovery"), for which an angular dependence is also observed (not shown here). However, the "recovered" spectrum differs from the "Initial" one.

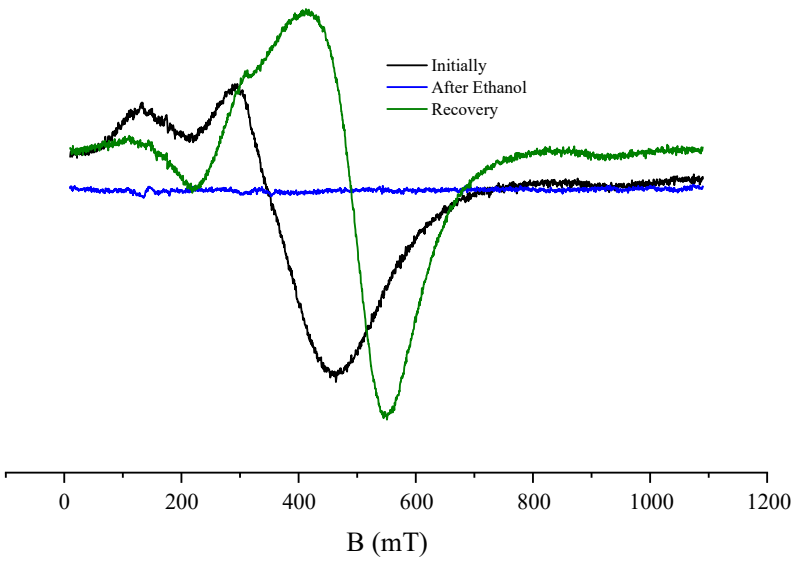

Figure 7. Room-temperature FMR spectra of CoSO-2h_av sample for the orientation of magnetic field perpendicular to the sample plane recorded before (black curve) and after (blue curve) storage of

 doi:10.20944/preprints202401.0296.v1

sample in ethanol medium. The green curve represents the FMR spectrum after the vacuum annealing of sample stored in ethanol.

3.6. Two magnetic phases in Co-ions heavily implanted SnO_2 films

Based on the abovementioned peculiarities in the magnetic properties of Co-ions implanted SnO_2 films at various temperatures of substrates as well as the XRD and the XPS results, we suppose the following explanation of the experimental data. The difference in magnetic properties of the samples is due to the various sources of ferromagnetism in them. Indeed, according to the XPS results, after the implantation at room temperature, cobalt atoms are predominantly in the metallic state, i.e., form metallic nanoparticles, which are responsible for the room temperature ferromagnetism. At the same time, after the implantation at the elevated temperature, the content of metallic Co atoms is sufficiently less and the implanted cobalt ions are mainly in the 2+ valence state. We assume that these ions form magnetically ordered solid solution in the SnO_2 host and the room temperature ferromagnetism of the corresponding sample is mainly originated by this solid solution. Since all our samples are in a highly insulating state (surface resistance more than 50 MΩ), the mechanism of magnetic ordering of Co^{2+} ions in this solid solution cannot be associated with carrier-mediated exchange such as RKKY-Zener type interaction [30]. For insulating rutile-type oxide materials, such as SnO_2 and TiO_2, F-center-mediated (FC) exchange between paramagnetic 3d-metal ions is often discussed to explain the high Curie temperature ferromagnetism [4,5,9,31,32]. In FC exchange model the localized spins of the magnetic dopants (e.g. Co^{2+} ions in low-spin state with S=1/2) interact with each other by an indirect ferromagnetic exchange through electrons trapped by neighboring oxygen vacancies. Thus, the presence of a certain concentration of oxygen vacancies plays a crucial role in producing ferromagnetism according to FC exchange mechanism.

The above-suggested model of two magnetic phases in Co-ions heavily implanted SnO_2 films can explain the influence of annealing environment on the magnetic properties of samples. Under annealing in air, the Co^{2+} based magnetic solid solution is oxidized in the temperature region of ~570-730 K, but this state may be recovered by the following annealing in vacuum. Thus, the initial state may be almost recovered even after removing the ferromagnetic response by the annealing in air in the case of SnO_2 film implanted with Co ions at the elevated temperature. The magnetic Co nanoparticles are oxidized at higher temperatures, namely, in the temperature region of ~730-900 K, but they are cannot be recovered under vacuum annealing. Therefore, in the case of SnO_2 film implanted with Co ions at room temperature the ferromagnetism after the annealing in air cannot be fully recovered because it is impossible to recovery the oxidized Co nanoparticles in the used experimental conditions of vacuum annealing.

The chemical effect of alcohol on FMR spectra, as we suppose, is due to the high content of atomic oxygen in such chemical molecular solutions as alcohol, toluene and acetone [33]. When a sample is kept in alcohol, oxygen atoms from the solution diffuse into the implanted film and fill oxygen vacancies in the crystal lattice. Thereby, ferromagnetism is suppressed, since oxygen vacancies are mediators of indirect exchange between Co^{2+} ions and play a dominant role in the establishment of long-range magnetic order according to the FC exchange model. Note that subsequent pumping of the sample in a vacuum chamber does not restore ferromagnetism. This means that oxygen atoms from the alcohol, when penetrating the SnO_2 film, interacts with tin atoms and forms a chemical bond with them. Ferromagnetism in the Co-implanted film can only be recovered by a heating the sample in a vacuum at temperatures above 450 °C (720 K). We suppose that at these conditions, the chemical bond of oxygen with tin is loosened and the oxygen atoms may be removed from the matrix by their back diffusion from the film into vacuum.

4. Conclusions

In summary, epitaxial SnO_2 thin films with rutile structure were grown on C-cut Al_2O_3 substrates using the reactive magnetron sputtering and subsequent high-temperature annealing in air. Then, 40 keV Co^+ ions were implanted into SnO_2 films at different temperature of substrate with a high concentration reaching a mean level of 12- 14 at.%. The microstructure and magnetic properties of

the heavily Co ions implanted SnO_2 films were investigated in detail. The Co implant was found in the mixed valence state: both in the form of metal Co^0 atoms and Co^{2+} ions; they are distributed non-homogenously in the implanted region of SnO_2 films. All Co-implanted SnO_2 films reveal room-temperature ferromagnetism with clearly defined magnetic hysteresis loops in in-plane geometry. It was shown that both the saturation magnetization (M_s) and the coercive field (H_c) strong depend on the substrate temperature during implantation. In particular, an unusually wide magnetic hysteresis loops with M_s~0.55 μB/Co and H_c ~ 2.5 kOe were observed in SnO_2 films implanted with cobalt at room temperature of substrate. To the best of our knowledge, such value of H_c have not been reported yet for Co-doped SnO_2 systems. Moreover, the processes of reduction and then recovery of ferromagnetism as a result of sequential annealing of Co-implanted films in air and then in vacuum, as well as the chemical effect of ethanol on FMR spectra were observed for the first time. These observations indicate a crucial role of oxygen vacancies in establishment of ferromagnetism in Co-implanted SnO_2 films. A model of the formation of two magnetic phases (Co nanoparticles and a magnetically isotropic solid solution of Co^{2+} ions) which are located at the different depth in Co ions heavily implanted SnO_2 films was used to explain the observed magnetic properties. However, additional investigations by high-resolution transmission electron microscopy are needed to verify the proposed two-phase model of ferromagnetism in Co-implanted SnO_2 films.

Supplementary Materials: The following supporting information can be downloaded at the website of this paper posted on Preprints.org, **Figure S1:** SEM images and EDX spectra of the surface of SnO_2 film before and after implantation of Co ions with the fluence of 1.0×10^{17} ion/cm^2; **Figure S2:** SEM image of the surface of SnO2 film after implantation of Ar ions with the fluence of 1.0×10^{17} ion/cm^2; **Figure S3:** AFM images of the surface of SnO_2 film before and after implantation of Co ions with the fluence of 1.0×10^{17} ion/cm^2; **Figure S4:** ^{119}Sn Mössbauer spectra of the epitaxial SnO_2 film on C-cut Al2O3 substrate before and after the implantation with 40 keV Co+ ions with the fluence of 1.0×10^{17} ion/cm^2; **Figure S5:** High resolution XPS spectra of Sn3d, O1s and Co2p binding energy regions for both as-prepared and Co ions implanted SnO_2 films.

Author Contributions: Conceptualization, R.I.K. and A.L.Z.; methodology, R.I.K. and A.L.Z.; validation, R.I.K. and A.L.Z.; formal analysis, R.I.K. and A.L.Z.; investigation, R.I.K., A.I.G., I.R.V., A.A.S., N.M.L., A.G.K., D.M.K., V.V.B., A.L.Z.; resources, R.I.K.; data curation, R.I.K.; writing—original draft preparation, R.I.K. and A.L.Z.; visualization, R.I.K., A.I.G., I.R.V. and A.L.Z.; supervision, R.I.K.; project administration, R.I.K.; funding acquisition, R.I.K. All authors have read and agreed to the published version of the manuscript.

Funding: The study was supported by the Russian Science Foundation (project number 22-19-00712, https://rscf.ru/project/22-19-00712/).

Data Availability Statement: The data presented in this study are available on request from the corresponding author. The data are not publicly available due to privacy restrictions.

Acknowledgments: Authors greatly acknowledge V.I. Nuzhdin and V.F. Valeev (from Zavoisky Physical-Technical Institute, FRC Kazan Scientific Centre of RAS, Russia) for help in ion implantation experiments. XPS measurements were taken under the Kazan Federal University Strategic Academic Leadership Program (PRIORITY-2030).

Conflicts of Interest: The authors declare no conflict of interest. The funders had no role in the design of the study; in the collection, analyses, or interpretation of data; in the writing of the manuscript; or in the decision to publish the results.

References

1. Dalapati, G. K.; Sharma, H.; Guchhait, A.; Chakrabarty, N.; Bamola, P.; Liu, Q.; Saianand, G.; Sai Krishna, A. M.; Mukhopadhyay, S.; Dey, A.; et al. Tin Oxide for Optoelectronic, Photovoltaic and Energy Storage Devices: A Review. *Journal of Materials Chemistry A*, **2021**, *9*, 16621–16684. https://doi.org/10.1039/d1ta01291f.
2. Worku, Y.; Sahu, D. R.; Srinivasu V. V. Ferromagnetism in SnO_2 Doped with Transition Metals (Fe, Mn and Ni) for Spintronics Application: A Review of Experimental Status. In *Magnetic Materials and Magnetic Levitation*; Sahu, D.R., Stavrou, V.N. Eds.; IntechOpen: Rijeka, Croatia, 2020; Chapter 7, pp. 1–14. https://doi.org/10.5772/intechopen.90902.
3. Fitzgerald, C. B.; Venkatesan, M.; Dorneles, L. S.; Gunning, R.; Stamenov, P.; Coey, J. M. D.; Stampe, P. A.; Kennedy, R. J.; Moreira, E. C.; Sias, U. S. Magnetism in Dilute Magnetic Oxide Thin Films Based On SnO_2. *Physical Review B*, **2006**, *74*, 115307. https://doi.org/10.1103/physrevb.74.115307.

4. Liu, X. F.; Sun, Y.; Yu, R. H. Role of Oxygen Vacancies in Tuning Magnetic Properties of Co-Doped SnO2 Insulating Films. *Journal of Applied Physics*, **2007**, *101*, 123907. https://doi.org/10.1063/1.2747591 .
5. Zuo, Y.; Ge, S.; Zhao, Y.; Zhou, X.; Xiao, Y.; Zhang, L. Room Temperature Ferromagnetism of $Sn_{1-x}Co_xO_{2-\delta}$ Films Fabricated by Sol-Gel Method. *Journal of Applied Physics*, **2008**, *104*. 023905. https://doi.org/10.1063/1.2956693.
6. Borges, P. D.; Scolfaro, L. M. R.; Alves, H. W. L.; da Silva, E. F., Jr; Assali, L. V. C. Study of the Oxygen Vacancy Influence on Magnetic Properties of Fe- and Co-Doped SnO_2 Diluted Alloys. *Nanoscale Research Letters*, **2012**, *7*, 540. https://doi.org/10.1186/1556-276x-7-540.
7. Ryssel, H.; Ruge, I. *Ionenimplantation*; Teubner: Stuttgart, Germany, 1978; 366p.
8. Heo, Y. W.; Kelly, J.; Norton, D. P.; Hebard, A. F.; Pearton, S. J.; Zavada, J. M.; Boatner, L. A. Effects of High Dose Ni, Fe, Co, and Mn Implantation into SnO_2. *Electrochemical and Solid-State Letters*, **2004**, *7*, G309. https://doi.org/10.1149/1.1814596.
9. Schoenes, J.; Pelzer, U.; Menzel, D.; Franke, K.; Ludwig, F.; Schilling, M. Ferromagnetism in Fe and Co-implanted SnO_2 Films. *Physica Status Solidi C*, **2006**, *3*, 4115–4118. https://doi.org/10.1002/pssc.200672819 .
10. Menzel, D.; Awada, A.; Dierke, H.; Schoenes, J.; Ludwig, F.; Schilling, M. Free-Carrier Compensation in Ferromagnetic Ion-Implanted SnO2:Co. *Journal of Applied Physics*, **2008**, *103*, 07D106. https://doi.org/10.1063/1.2830796.
11. Fairley, N.; Fernandez, V.; Richard-Plouet, M.; Guillot-Deudon, C.; Walton, J.; Smith, E.; Flahaut, D.; Greiner, M.; Biesinger, M.; Tougaard, S.; et al. Systematic and Collaborative Approach to Problem Solving Using X-Ray Photoelectron Spectroscopy. *Applied Surface Science Advances*, **2021**, *5*, 100112. https://doi.org/10.1016/j.apsadv.2021.100112.
12. Iassonov, P.G.; Nourgaliev, D.K.; Bourov, B.V.; Heller, F. A modernized coercivity spectrometer. *Geologica Carpathica*, **1998**, *49*, 224–226.
13. Kosareva, L. R.; Shcherbakov, V. P.; Nurgaliev, D. K.; Nurgalieva, N. G.; Sycheva, N. K.; Antonenko, V. V.; Kuzina, D. M.; Evtyugin, V. G. Periodization of Holocene Climatic Cycles Based on Synchronous Variations in the Magnetic and Geochemical Parameters of the Sediments of Lake Bolshoe Yarovoe (Southwestern Siberia). *Russian Geology and Geophysics*, **2020**, 61, 723–737. https://doi.org/10.15372/rgg2019148.
14. Zhang, M.; Xu, M.; Li, M.; Zhang, Q.; Lu, Y.; Chen, J.; Li, M.; Dai, J.; Chen, C.; He, Y. SnO_2 Epitaxial Films with Varying Thickness on C-Sapphire: Structure Evolution and Optical Band Gap Modulation. *Applied Surface Science*, **2017**, 423, 611–618. https://doi.org/10.1016/j.apsusc.2017.06.250.
15. Liu, H.-G.; Zheng, W.-C.; He, L. EPR g Factors and Defect Structures for Co^{2+} Ions at the Substitutional and Interstitial Sites of SnO_2 Lattice. *Radiation Effects and Defects in Solids*, **2008**, 163, 1–6. https://doi.org/10.1080/10420150701688610.
16. Wang, H.; Yan, Y.; Mohammed, Y. Sh.; Du, X.; Li, K.; Jin, H. First-Principle Study of Magnetism in Co-Doped SnO_2. *Journal of Magnetism and Magnetic Materials*, **2009**, 321, 337–342. https://doi.org/10.1016/j.jmmm.2008.09.020.
17. Shannon, R. D. Revised Effective Ionic Radii and Systematic Studies of Interatomic Distances in Halides and Chalcogenides. *Acta Crystallographica Section A*, **1976**, 32, 751–767. https://doi.org/10.1107/s0567739476001551.
18. Zinnatullin, A. L.; Petrov, A. V.; Yusupov, R. V.; Valeev, V. F.; Khaibullin, R. I.; Vagizov, F. G. Unusual Compositions of Fe-Nb Alloy Precipitates in Iron-Implanted $LiNbO_3$. *Magnetochemistry*, **2023**, 9, 121. https://doi.org/10.3390/magnetochemistry9050121.
19. Drouin, D.; Couture, A.R.; Joly, D.; Tastet, X.; Aimez, V.; Gauvin, R. CASINO V2.42—A Fast and Easy-to-use Modeling Tool for Scanning Electron Microscopy and Microanalysis Users. *Scanning* **2007**, *29*, 92–101. https://doi.org/10.1002/sca.20000.
20. Ziegler, J.F.; Ziegler, M.D.; Biersack, J.P. SRIM—The Stopping and Range of Ions in Matter. *Nucl. Instrum. Methods Phys.Res. Sect. B Beam Interact. Mater. At.* **2010**, *268*, 1818–1823. https://doi.org/10.1016/j.nimb.2010.02.091
21. Achkeev, A. A.; Khaibullin, R. I.; Tagirov, L. R.; Mackova, A.; Hnatowicz, V.; Cherkashin, N. Specific Features of Depth Distribution Profiles of Implanted Cobalt Ions in Rutile TiO_2. *Physics of the Solid State*, **2011**, 53, 543–553. https://doi.org/10.1134/s1063783411030024.
22. Powell, C. X-Ray Photoelectron Spectroscopy Database XPS,Version 4.1, *NIST Standard Reference Database 20*, **1989**. https://doi.org/10.18434/T4T88K.
23. Biesinger, M. C.; Payne, B. P.; Grosvenor, A. P.; Lau, L. W. M.; Gerson, A. R.; Smart, R. St. C. Resolving Surface Chemical States in XPS Analysis of First Row Transition Metals, Oxides and Hydroxides: Cr, Mn, Fe, Co and Ni. *Applied Surface Science*, **2011**, 257, 2717–2730. https://doi.org/10.1016/j.apsusc.2010.10.051.
24. Kılıç, Ç.; Zunger, A. Origins of Coexistence of Conductivity and Transparency in SnO_2. *Physical Review Letters*, **2002**, 88. https://doi.org/10.1103/physrevlett.88.095501.

25. Xiong, Y.; Lin, Y.; Wang, X.; Zhao, Y.; Tian, J. Defect Engineering on SnO_2 Nanomaterials for Enhanced Gas Sensing Performances. *Advanced Powder Materials*, **2022**, 1, 100033. https://doi.org/10.1016/j.apmate.2022.02.001.
26. Joshi, J. P.; Bhat, S. V. On the Analysis of Broad Dysonian Electron Paramagnetic Resonance Spectra. *Journal of Magnetic Resonance*, **2004**, 168, 284–287. https://doi.org/10.1016/j.jmr.2004.03.018.
27. Virtanen, P.; Gommers, R.; Oliphant, T. E.; Haberland, M.; Reddy, T.; Cournapeau, D.; Burovski, E.; Peterson, P.; Weckesser, W.; Bright, J.; et al. SciPy 1.0: Fundamental Algorithms for Scientific Computing in Python. *Nature Methods*, **2020**, 17, 261–272. https://doi.org/10.1038/s41592-019-0686-2.
28. Okay, C.; Vakhitov, I. R.; Valeev, V. F.; Khaibullin, R. I.; Rameev, B. Magnetic Resonance Study of Fe-Implanted TiO_2 Rutile. *Applied Magnetic Resonance*, **2017**, 48, 347–360. https://doi.org/10.1007/s00723-017-0868-y.
29. Kazan, S.; Mikailzade, F. A.; Şale, A. G.; Maksutoğlu, M.; Acikgoz, M.; Khaibullin, R. I.; Khalitov, N. I.; Gatiiatova, Ju. I.; Valeev, V. F. Magnetic Properties of Co-Implanted $BaTiO_3$ Perovskite Crystal. *Physical Review B*, **2010**, 82. https://doi.org/10.1103/physrevb.82.054402.
30. Zener, C. Interaction Between The *d* Shells in the Transition Metals. *Physical Review*, **1951**, 81, 440–444. https://doi.org/10.1103/physrev.81.440.
31. Coey, J. M. D.; Douvalis, A. P.; Fitzgerald, C. B.; Venkatesan, M. Ferromagnetism in Fe-Doped SnO_2 Thin Films. *Applied Physics Letters*, **2004**, 84, 1332–1334. https://doi.org/10.1063/1.1650041.
32. Khaibullin, R. I.; Ibragimov, Sh. Z.; Tagirov, L. R.; Popok, V. N.; Khaibullin, I. B. Formation of Anisotropic Ferromagnetic Response in Rutile (TiO_2) Implanted with Cobalt Ions. *Nuclear Instruments and Methods in Physics Research Section B: Beam Interactions with Materials and Atoms*, **2007**, 257, 369–373. https://doi.org/10.1016/j.nimb.2007.01.064.
33. Shchukarev, S. A.; Tolmacheva, T. A. Solubility of Oxygen in Ethanol-Water Mixtures. *Journal of Structural Chemistry*, **1968**, 9, 16–21. https://doi.org/10.1007/bf00744018.